International Soil and Water Conservation Research

# Fingerprinting using compound-specific δ13C of n-alkanes indicates the relative importance of paddy fields as a temporary secondary source of watershed sediment loss

--Manuscript Draft--

| | |
|---|---|
| **Manuscript Number:** | |
| **Article Type:** | Research Paper |
| **Section/Category:** | Soil erosion and control |
| **Keywords:** | Source apportionment; Sediment fingerprinting; Biomarkers; Compound-specific stable isotopes; Heterogenous landscape |
| **Corresponding Author:** | Qiang Tang<br><br>CHINA |
| **First Author:** | Qiang Tang |
| **Order of Authors:** | Qiang Tang |
| | Fangxin Chen |
| | Guangyu Zhu |
| | Xiubin He |
| | Jie Wei |
| | Yusheng Zhang |
| | Hari Upadhayay |
| | Adrian Joynes |
| | Adrian Collins |
| **Abstract:** | Sediment fingerprinting generates reliable sediment provenance information which supports policy or practical strategies for catchment sediment management. But the approach remains challenging in areas with complex landscape configuration. This investigation evaluated the seasonality of biomarker signatures and their variability among particle size fractions, and accordingly apportioned target time-integrated suspended sediment to land-use based sources in an intensive farming watershed with mosaic land use patch configurations and crop-specific farming practices. Source materials (i.e., topsoil) from dry croplands, paddy fields and citrus orchards were sampled, and time-integrated suspended sediment was collected at the watershed outlet. The absolute concentrations and compound-specific δ13C of long-chain saturated n-alkanes (C23-C33) were determined for two absolute particle size fractions (i.e., <25 μm and 25-63 μm). The δ13C of monomeric n-alkanes displayed no significant variabilities between the particle aize fractions nor across the whole sampling period. The MixSIAR Bayesian model was employed to quantify sediment source contributions. Due to human activities, paddy fields have become an important sediment source, but dry farmland remains the largest contributor. Based on sediment source information for the study watershed, a range of measures such as soil virginization, returning straw to fields, and pasture cultures in orchards are recommended. |
| **Suggested Reviewers:** | Valentine Golosov<br>Lomonosov Moscow State University<br>gollossov@gmail.com |
| | Xingwu Duan<br>Yunnan University<br>xwduan@ynu.edu.cn |
| **Opposed Reviewers:** | |

**15th August, 2024**
**Editor-In-Chief**
**International Soil and Water Conservation Research**

Dear Editor,

Enclosed, please find a manuscript entitled “Fingerprinting using compound-specific $\delta^{13}C$ of n-alkanes indicates the relative importance of paddy fields as a temporary secondary source of watershed sediment loss”, which has been nominated for the WASWAC Youth Outstanding Paper Award 2024 (YOPA ID: YOPA-2024-037) and is now submitted to *International Soil and Water Conservation Research* for publication.

The Three Gorges Reservoir Area represents a hot-spot region for soil erosion due to mountainous and hilly landform, frequent erosive rainfall storms, and intensive surface land disturbance by human activities, where soil conservation is of utmost importance in terms of its potential adverse consequences to receiving freshwater impounded by the dam. Sediment fingerprinting generates reliable sediment provenance information which supports policy or practical strategies for catchment sediment management. But the approach remains challenging in areas with complex landscape configuration. This investigation evaluated the seasonality of biomarker signatures and their variability among particle size fractions, and accordingly apportioned target time-integrated suspended sediment to land-use based sources in an intensive farming watershed with mosaic land use patch configurations and crop-specific farming practices. Source materials (i.e., topsoil) from dry croplands, paddy fields and citrus orchards were sampled, and time-integrated suspended sediment was collected at the watershed outlet. The absolute concentrations and compound-specific δ13C of long-chain saturated n-alkanes (C23-C33) were determined for two absolute particle size fractions (i.e., <25 μm and 25-63 μm). The $\delta^{13}C$ of monomeric n-alkanes displayed no significant variabilities between the particle aize fractions nor across the whole sampling period. The MixSIAR Bayesian model was employed to quantify sediment source contributions. Due to human activities, paddy fields have become an important sediment source, but dry farmland remains the largest contributor. Based on sediment source information for the study watershed, a range of measures such as soil virginization, returning straw to fields, and pasture cultures in orchards are recommended.

This contribution is an original study that has not been published elsewhere and is not under consideration by any other journals. If accepted, it will not be published elsewhere in the same form, in English or in any other language, including electronically without the written consent of the copyright holder. All authors have read and approved the manuscript in the form submitted, take responsibility for its content, and agree to this submission.

We respectfully suggest that the following individuals would be suitable peer reviewers based on their expertise in the field:

Valentin Golosov
Moscow University, Russia
E-mail: gollossov@gmail.com

Xingwu Duan
Yunnan University
E-mail: xwduan@ynu.edu.cn

We thank you very much for considering this work and look forward to your response.

Yours sincerely,

Qiang Tang (on behalf of the authorship team)
Chongqing Jinfo Mountain Karst Ecosystem National Observation and Research Station
School of Geographical Sciences, Southwest University
No. 2, Tiansheng Road, Beibei District, Chongqing 400715, China
Tel.: +86-23-68367680;
Fax: +86-23-68253912;
E-mail: qiangtang@swu.edu.cn

**Declaration of conflict of interest**

The authors declare that they have no conflict of interest.

# Fingerprinting using compound-specific $\delta^{13}C$ of n-alkanes indicates the relative importance of paddy fields as a temporary secondary source of watershed sediment loss


## Abstract

Sediment fingerprinting generates reliable sediment provenance information which supports policy or practical strategies for catchment sediment management. But the approach remains challenging in areas with complex landscape configuration. This investigation evaluated the seasonality of biomarker signatures and their variability among particle size fractions, and accordingly apportioned target time-integrated suspended sediment to land-use based sources in an intensive farming watershed with mosaic land use patch configurations and crop-specific farming practices. Source materials (i.e., topsoil) from dry croplands, paddy fields and citrus orchards were sampled, and time-integrated suspended sediment was collected at the watershed outlet. The absolute concentrations and compound-specific $\delta^{13}C$ of long-chain saturated n-alkanes ($C_{23}$-$C_{33}$) were determined for two absolute particle size fractions (i.e., <25 μm and 25-63 μm). The $\delta^{13}C$ of monomeric n-alkanes displayed no significant variabilities between the particle aize fractions nor across the whole sampling period. The MixSIAR Bayesian model was employed to quantify sediment source contributions. Due to human activities, paddy fields have become an important sediment source, but dry farmland remains the largest contributor. Based on sediment source information for the study watershed, a range of measures such as soil virginization, returning straw to fields, and pasture cultures in orchards are recommended.


**Keywords**: Source apportionment; Sediment fingerprinting; Biomarkers; Compound-specific stable isotopes; Heterogenous landscape

## 1. Introduction

The global soil denudation system has been severely disrupted by expanding and intensifying human activities during the Anthropocene, such as large-scale deforestation, land clearance and reclamation, farming practices, infrastructure construction, dam operations, and urbanization (Jenny et al., 2019). Consequently, global modern soil erosion patterns have been unprecedently complicated by constant human modification of the earth, climate change impacts, and conservation actions over recent decades (Borrelli et al., 2020; Wuepper et al., 2020). Suspended sediment arising from the mobilization of eroded materials from distal upland sources or proximal within-channel sources acts as an essential structural and functional component of river systems (Apitz, 2012). Its transport dynamics influence the extent and intensity of geomorphological evolution (e.g., aggregation or degradation) of fluvial channels, and determines the continent-ocean delivery of terrestrial materials along river continuums (Ludwig et al., 1996; Walling, 2006). More recently, growing awareness has been directed to the ecological significance of suspended sediment in rivers since fine-grained particle dispersal acts as a critical vector for redistributing contaminants (e.g., nutrients, carbon, inorganic metals, and organic compounds, etc.), which deliver complicated detrimental consequences for water quality, river ecology and aquatic ecosystem health more generally (Walling and Fang, 2003).

Acquiring reliable sediment provenance information is critical for informing appropriate soil conservation policies or measures but is difficult to obtain in view of the diffuse nature of sediment mobilization and delivery and their concomitant variability in space and time. Sediment fingerprinting provides a useful approach for quantifying the relative contributions of sampled sources to target sediments at catchment scale via establishing a direct link between the tracer signatures of sources and sediment materials (Collins and Walling, 2004). The applicability of the approach to catchments with contrasting environmental contexts has been improved through the testing and adoption of an increasing number of tracers represented by inherent soil properties, including physical properties (Krein et al., 2003; Martinez-Carreras et al., 2010; Pulley et al., 2018), fallout radionuclides (Pulley et al., 2019), mineral magnetism (Kayvantash et al., 2017; Rowntree et al., 2017), stable isotopes (Fox and Papanicolaou, 2008; Mabit et al., 2018), geochemical elements (Chen et al., 2016; Chen et al., 2019), optical tracers (Verheyen et al., 2014; Tiecher et al., 2016) and biomarkers (Blake et al., 2012; Hancock and

55 Revill, 2013; Chen et al., 2016; Chen et al., 2017). In some cases, the diversity of properties
56 available has provided a basis for generating estimates of the contributions from a wide range
57 of sources (e.g., spatial locations, erosion processes, land use categories or landscape units).
58 Equally, the temporal coverage and resolution of the information provided by sediment
59 fingerprinting is flexible on the basis of using a variety of targeted sediment sampling strategies
60 including, for example, snapshot suspended sediment sampling throughout the hydrographs of
61 individual storm events, time-integrated suspended sediment sampling, channel bed sediment
62 remobilization or the coring of long-term floodplain deposits (Owens et al., 1999), or historical
63 sedimentary archives preserved in lakes or reservoirs (Ben Slimane et al., 2013; Kim et al.,
64 2013; Fang, 2015; Chen et al., 2017; Huang et al., 2019). Alongside the increasing number of
65 case study applications, the most recent work has revisited the major assumptions
66 underpinning sediment fingerprinting to improve the reliability of the source estimates obtained,
67 for example, reexamining the conservative behaviour or diagnostic ability of both traditional and
68 novel tracers by evaluating the spatial and temporal within-source variability of tracer signatures
69 (Collins et al., 2019; Du and Walling, 2017; Reiffarth et al., 2016; Reiffarth et al., 2019), or
70 testing the appropriateness of conventional source classification schemes and providing
71 methodologies for refining source classification strategies (Zhou et al., 2016; Pulley et al., 2017;
72 Vercruysse and Grabowski, 2018).

73 One of the most recent advances concerns increasing adoption of compound-specific
74 stable isotope (CSSI) tracers since, in some catchments, these have the potential to generate
75 reliable estimates of the relative contributions of land use-based sources to sampled target
76 sediment. The basic technological premise here lies in the fact that land use or vegetation cover
77 can imprint soil with a specific $\delta^{13}C$ signature through organic matter inputs associated with
78 litter decomposition (Upadhayay et al., 2017). Biomarkers, including for example, long-chain
79 saturated n-alkanes with a strong odd/even predominance derived from terrestrial higher plants,
80 are found to be highly resistant to microbial decomposition and persist in the environment
81 alongside sediment mobilization and storage, thereby permitting their use as tracers for
82 apportioning sediment contributions from land use-based or plant/crop-specific sources (Blake
83 et al., 2012; Cooper et al., 2015). Here, however, as landscape fragmentation can potentially
84 result in greater within-source variability of tracer signatures, the diagnostic power of

biomarkers needs to be evaluated carefully (Reiffarth et al., 2019; Upadhayay et al., 2020).

A variety of fingerprint tracers has been employed according to the physical environmental context of the research catchment in question (e.g., different geologies, land uses, etc.). For example, in areas where lithology controls erosion, geochemical fingerprints are usually used in sediment fingerprinting framework (Krein et al., 2003; Fox and Papanicolaou, 2008; Martinez-Carreras et al., 2010; Verheyen et al., 2014; Tiecher et al., 2016; Rowntree et al., 2017; Mabit et al., 2018; Pulley et al., 2019); whereas in situations where geological variations are small or where different land uses span geological boundaries, biomarkers are increasingly shortlisted as potentially useful fingerprint properties (Blake et al., 2012; Hancock and Revill, 2013; Chen et al., 2016; Tiecher et al., 2016; Chen et al., 2017; Mabit et al., 2018). Alongside the increasing number of tracer properties applied in source fingerprinting studies, the number and structures of un-mixing models for estimating source proportions has also expanded. Here, models are either frequentist or Bayesian but can also differ within either category with regards the inclusion or exclusion or various correction factors and weightings (Collins et al., 1997a; Collins et al., 2017). Whereas as early studies typically used the <63 μm fraction regardless of catchment setting or tracer selection (Collins et al., 1997a; Collins et al., 2017), it is now recommended that careful attention be directed towards adoption of the most relevant size fraction for both (Collins et al., 2017). In some cases, this has resulted in the use of the <10 μm fraction (Theuring et al., 2015).

Sediment source fingerprinting in many previous cases was undertaken in homogeneous landscapes with relatively larger field sizes and simple farming practices. But, in China, most landscapes in the hilly and mountainous regions have been heavily fragmented by mosaic land use patches under the household-based farming system, where crop selection has been diversified and corresponding farming practices differ substantially. Paddy fields represent the dominant land use in south China which was traditionally viewed as a temporary sediment sink, but, from a longer-term perspective, could be a secondary sediment source resulting from the remobilization of deposited sediment. Fragmented landscapes with complex land use patterns and histories, such as those in many parts of China, potentially present a particular challenge to the capacity to identify and apply diagnostic source fingerprints (Tang et al., 2019). In the specific case of testing biomarkers in such settings, two issues requiring further investigation

concern the comparison of CSSI source apportionment using different particle size fractions and the assumption that biomarkers remain stable over the long-term (Hancock and Revill, 2013; Chen et al., 2017). To this end, this investigation examined the temporal variability of biomarker tracers closely related to land use and vegetation cover and their variability among different particle size fractions. In so doing, we also quantified the relative contributions of land-use based source units to target time-integrated suspended sediment samples in a typical hilly farming landscape. Paddy fields are a popular land use practice for rice planting in the humid region of southern China, and although these have conventionally been viewed as sediment sinks along hydrological pathways, they were assumed to be a secondary sediment source in our study.

## 2. Materials and methods

### *2.1 Site description*

The Three Gorges Reservoir Area is spread across the transitional area from the Sichuan depression to middle-lower Yangtze plain (Fig. 1a). The landforms are characterized by hilly landscapes in the upper and middle reaches, while mountains and valleys prevail in the lower reaches. The climate is dominated by humid temperate monsoons, with mean annual rainfall being 1200mm. Land use is closely related to topography and human occupation. Forests and grasslands prevail in the mountainous areas where population density is low, while cropping land is predominantly in the hilly areas with high population density. Agriculture is managed by small-sized household crop farms, mainly consisting of dry croplands and paddy fields. Significant land use change has taken place due to dam construction, urbanization, infrastructure expansion, as well as a reforestation campaign, wherein arable lands have been converted to woodland or urban areas. Human relocation and water impoundment arising from the dam construction have elevated land resource scarcity, leading to the expansion of farming on marginal range lands and more intensive cultivation practices. The Three Gorges Reservoir Area has exhibited high rates of soil erosion, which seriously threaten sustainable agricultural land use, as well as aquatic ecosystem health. Soil conservation is thus a high management priority aiming to prevent the world's largest reservoir from experiencing rapid sedimentation and water quality deterioration from diffuse contaminant export associated with sediment

mobilization and delivery (Fu et al., 2010). This region is earmarked as a high priority for hillslope soil conservation, given the essential role of sediment transport in exporting diffuse contaminants, which would threaten the environmental quality and ecosystem health of the large reservoir, as well as rapid sedimentation eliminating the operational capacity of the reservoir.

This study was conducted in the Xinzheng catchment (0.25 $km^2$) in Zhong County in the central Three Gorges Reservoir Area (Fig. 1b). The catchment landform is hilly with elevations ranging from 209 to 322 m a.s.l. The purple soil, which is developed from the Trias-Cretaceous system of sedimentary rocks and classified as Regosols in the FAO Taxonomy or Entisols in the USDA Taxonomy (He et al., 2009), is highly susceptible to rainfall detachment and runoff dispersal. Annual average rainfall is 1172 mm and a major proportion occurs in the rainy season from May to September. Catchment land use consists of dry croplands (36%), citrus orchards (35%), paddy fields (19%), rural residences (5.7%), paved roads (1.9%), water (1.7%) and exposed bare rock (0.7%) (Fig. 1c). The catchment uplands are predominantly occupied by sloping or terraced dry croplands (Fig. 2a) which are intensively cultivated throughout the year. Canola (*Brassica napus* L.) and cabbage (*Brassica oleracea* L. var. capitata L.) are key winter crops while maize (*Zea mays* L.) and sweet potato (*Ipomoea batatas* (L.) Lam.) are important summer crops. Citrus orchards situated along the middle slopes were converted from dry croplands more than 15 years ago (Fig. 2c). Citrus orchards have experienced the least intensity of land disturbance as no tillage is practiced but receive large inputs of agricultural chemicals such as pesticides, herbicides, and fertilizers, and are therefore likely to be a high-risk source for diffuse pollution generation. Paddy fields distributed on the valley floors where rice is planted during April to August (Fig. 2b) remain uncultivated and impounded with shallow water in the winter season, but undergo mechanical tillage before rice reseeding in April. There is a small pond in the upper section of the study catchment, receiving runoff from upstream (Fig. 2a).

### *2.2 Sampling strategies*

Catchment-wide generic sediment sources were classified *a priori* as dry croplands, citrus orchards, and paddy fields. Mosaic bare rock, woodland, rural residences, paved roads, and

175 water were not prescribed as potential sediment sources in this study given their relatively minor
176 importance to soil erosion and sediment supply. Each topsoil (0-2 cm) source sample was
177 composed of 10 random subsamples collected in the immediate vicinity using a stainless-steel
178 corer. Composite samples were collected to improve the spatial representativeness of the
179 source material samples. Six composite topsoil samples were collected for each source
180 category (18 source samples in total) in late March 2017 before the ploughing of the paddy
181 fields and rice reseeding, while 14 composite topsoil samples were taken (42 source samples
182 in total) in late April 2018 after paddy field ploughing and rice reseeding.
183 Time-integrated suspended sediment was collected at the catchment outlet over the period
184 from March 2017 to September 2018 using four independent Phillips samplers (Phillips et al.,
185 2000). All samplers were deployed in May 2017 during the first field campaign. The first sample
186 retrieval was conducted in July 2017 when one composite sample was obtained by mixing four
187 independent samples. For each suspended sediment sampling period, large organic detritus
188 was removed manually, and sediment was settled in a dark cool room for 7–10 days. Excess
189 water was siphoned off without disturbing the settled sediment. There were nine samples
190 collected in 2017 and a further six samples in 2018 (Table 1).
191
192 *2.3 Laboratory analysis*
193 Both source and target time-integrated suspended sediment samples were freeze-dried,
194 manually disaggregated, and sieved through a 63 μm mesh. To select the most appropriate
195 particle size fraction for the source fingerprinting work, time-integrated suspended sediment
196 samples were analyzed for absolute grain size with a Malvern Mastersizer laser diffraction
197 granulometer, following pre-treatment with hydrogen peroxide and ultrasonic dispersion post
198 the application of sodium hexametaphosphate as a dispersal agent. This analysis indicated that
199 the $d_{90}$ of the absolute particle size of the target suspended sediment samples ranged from 41-
200 60 μm, with a corresponding average of 48 μm and a median of 49 μm. Because it is also
201 informative to consider any potential effects of tracer distribution within particle size fractions of
202 source and target sediment samples, especially where the $d_{90}$ is reasonably coarse, all samples
203 were separated into <25 μm and 25-63 μm fractions. This provided a basis for comparing
204 source fingerprinting results for two absolute particle size fractions.

Sample extraction and n-alkanes fractionation were performed using the following procedure. Approximately 10 g of sample was weighed into a thimble and soxhlet extracted with 250 ml of dichloromethane (DCM): acetone (9:1, v/v) for 24 h. Before the extraction, a 100 ul of 1 mg/ml $C_{19}$ and $C_{34}$ n-alkane internal standard was added. The total lipid extract (TLE) was evaporated to dryness using a rotatory evaporator (*Buchi*), then re-dissolved in 3 x 2 ml DCM: acetone (1:1), transferred to a vial and re-evaporated to dryness under a gentle stream of nitrogen ($N_2$) at 37 $^oC$. To obtain a neutral lipid extract (NL), the TLE was dissolved in a ml of chloroform, the 0.5 ml of the extract was eluted through an activated silica column 60A, particle size 35-70, (Fisher Scientific), with 5 ml of chloroform and then blown down to dryness with $N_2$. To obtain the hydrocarbon fraction containing the n-alkanes, the NL was dissolved in 2 ml hexane, 0.5 ml was eluted through another silica column with 4 ml of hexane and then blown down to dryness with $N_2$.

The absolute abundance of $C_{23}$-$C_{33}$ n-alkanes was quantified using an Agilent 7890A GC with a flame ionization detector (FID), 7963 autosampler and splitless injector at 300 $^oC$ (Agilent Technologies). Prior to analysis, the hydrocarbon fraction was re-dissolved in 2 ml of hexane and 100 ul transferred to a 2 ml vial. The oven programme was hold at 40 $^oC$ for 1 min, then ramp to 130 $^oC$ at 20 $^oC$ per minute, then 4 $^oC$ per minute to 300 $^oC$ and hold for 10 min. The GC column was an Agilent HP-5 (30 m x 320 μm x 0.250 μm) with helium carrier gas at a flow rate of 1 ml per minute. The odd n-alkanes ($C_{23}$-$C_{33}$) were initially identified by retention times and distinctive odd/even patterns. The concentrations were determined relative to the $C_{34}$ internal standard. The identity of the n-alkanes was confirmed using GC-MS. Here, the n-alkanes spectra were compared to those in the National Institute of Standards spectral library (NIST, US Gov.) and characteristic base peaks identified.

The compound-specific $\delta^{13}C$ signatures ($\delta^{13}C_{23}$, $\delta^{13}C_{25}$, $\delta^{13}C_{27}$, $\delta^{13}C_{29}$, $\delta^{13}C_{31}$, $\delta^{13}C_{33}$) were determined using a Finnigan Mat 6890 GC coupled to a Finnigan Mat Delta Plus IRMS via a Combustion III interface, with oxidation reactor containing platinum/copper oxide and nickel oxide at 940 $^oC$ (Thermo Fisher Scientific, Bremen, Germany). Samples were introduced using a PAL AS200 autosampler (CTC analytics, Switzerland) via splitless injector at 300 $^oC$ with helium carrier gas at 1.4 ml per minute. The oven programme was the same as above, but the column was a Varian CP-SIL 5CB (50 m x 320 μm x 0.12 μm) (Varian Inc. California, US). The

235 $\delta^{13}C$ ratio was determined relative to $CO_2$ reference gas of known $\delta^{13}C$ and N5.5 grade purity
236 (BOC, Guildford, UK) previously calibrated by Iso-Analytical. The reference gas was injected
237 directly to the source just prior to the n-alkane peaks of interest, and four times at the beginning
238 and end of each run. The $\delta^{13}C$ was expressed relative to Vienna Pee Dee Belemnite (VPDB).
239 During the runs, the known $\delta^{13}C$ values of the $C_{19}$ and $C_{34}$ internal standard (determined in
240 house) in the samples was monitored as well as running the n-alkane standards at the
241 beginning and end of each batch. The operation of the system was regularly checked using a
242 certified n-alkane compound mixture $C_{16}$-$C_{30}$ (Indianna State University, US) with variable $\delta^{13}C$
243 values over a range of concentrations. The $\delta^{13}C$ should be >1‰ from the reference value. The
244 stability and linearity of the system were better than 0.06‰. The $\delta^{13}C$ standard deviation from
245 the standards was ± 0.35‰.
246
247 *2.4 Sediment source fingerprinting procedure*
248 Prior to un-mixing source contributions to the target time-integrated suspended sediment
249 samples, tracer conservation was assessed using a bracket test. Selected conservative tracers
250 were then tested individually for their source discrimination efficiency using the Kruskal-Wallis
251 rank sum test (Collins et al., 1997b). Here, any properties returning a statistical significance of
252 P >0.05 were excluded from further analysis. Properties passing the Kruskal-Wallis test were
253 then used in a stepwise discriminant function analysis (DFA) to identify a composite set of
254 signatures for un-mixing modelling (Collins et al., 1997c). The estimation of the relative
255 contribution of each potential sediment source to the target time-integrated suspended
256 sediment samples was assessed with the concentration-dependent MixSIAR model
257 (Upadhayay et al., 2018a). This model has been widely used for un-mixing compound-specific
258 stable isotopes (CSSI) of odd long-chain n-alkanes ($C_{23}$-$C_{33}$). MixSIAR was implemented in the
259 R package linked to the JAGS 3.3.0 library for Bayesian data analysis using a Gibbs sampling
260 Markov chain Monte Carlo (MCMC) algorithm (Plummer, 2003) and a fractionation factor of
261 zero was used. The Markov Chain Monte Carlo (MCMC) parameters in MixSIAR were set as
262 follows: number of chains = 3, chain length = 5,000,000 (extreme), burn = 1,500,000, thin =500.
263 The convergence of un-mixing models was evaluated using the Gelman-Rubin diagnostic,
264 rejecting the model output if any variable was above 1, in which case the chain length was

increased. Furthermore, a diagnostic matrix plot of posterior source contributions was used to evaluate the quality of source discrimination. Density plots of the proportional source contributions are reported along with a mean, median and standard deviation. MixSIAR simulations were run by considering different levels of prior informativeness defined in this research as the sum of the prior input into the model. The input priors ranged from low informative priors in which the sum of the priors input was 1, medium informative priors in which the weight of the prior was set as the number of sources, to very informative priors in which the sum of the priors correspond to 100 (Upadhayay et al., 2018b).

## 3. Results

### *3.1 The behaviour of biomarker signatures among source categories and particle size fractions*

Source materials from paddy fields exhibited the highest n-alkane concentrations of 4863.8 ± 1116.2 ng/g in the <25 μm faction and 5855.9 ± 2294.3 ng/g in the 25-63 μm faction, followed by those from citrus orchards, with 5513.5 ± 3137.8 ng/g in the <25 μm fraction and 3999.8 ± 1241.4 ng/g in the 25-63 μm fraction. Dry croplands exhibited the lowest n-alkane concentrations of 2122.5 ± 793.6 ng/g in the 0-25 μm and 2447.5 ± 1506.3 ng/g in the 25-63 μm fraction. N-alkane concentrations were higher in the finer particle size fractions in the soil samples collected to characterize citrus orchards. However, in the case of samples collected to characterize the signatures of dryland farming and paddy fields, this trend was not exhibited (Fig. 3). All source soil samples showed obvious odd-number n-alkane predominance, wherein the dominant peaks were $C_{31}$, $C_{33}$ and $C_{29}$ in orange orchard samples, $C_{27}$, $C_{31}$ and $C_{29}$ in paddy field samples, and $C_{29}$, $C_{31}$ and $C_{33}$ in dry farmland samples. These three n-alkanes accounted for more than 60% of the total n-alkanes. Differences in the $\delta^{13}C$ of n-alkanes among the different sediment source categories were not obvious (Fig. 3). T tests was employed to examine the presence of any differences between the $\delta^{13}C$ of n-alkanes or n-alkane content of the two particle size fractions for each source category. These tests revealed some statistically significant differences for the paddy field and orange orchard sediment sources. On this basis, the <25 μm fraction was used to fingerprint sediment sources to minimize any particle size effects. Molecular biomarkers are potentially influenced by the conversion of organic matter and farming practices between years. We therefore tested for statistically significant differences

between the $\delta^{13}C$ of n-alkanes for the two sampling years (Table 2). The results indicated that there were no significant differences and, accordingly, we considered it appropriate to use the soil samples collected from each source in both 2017 and 2018 when estimating the proportional contributions to the time-integrated suspended sediment samples.

*3.2 Tracer selection and sediment source discrimination*

All six fingerprint properties taken forward in the data processing procedure returned a P value of <0.01 from the Kruskal-Wallis H test, with the H-values ranging from 9.59 to 33.52 (Table 3). Individually, the $\delta^{13}C$ of all odd-numbered n-alkanes returned statistically significant differences among the three potential sediment sources (P-value < 0.01; Table 4). DFA indicated that the discriminatory efficiency of the individual tracers ranged between 51.7% and 65.0%. The $\delta^{13}C_{25}$ was the only individual fingerprint property excluded from the final composite signature which yielded a discriminatory efficiency of 90% (Table 4). On this basis, a final composite signature combining $\delta^{13}C_{33}$, $\delta^{13}C_{23}$, $\delta^{13}C_{29}$, $\delta^{13}C_{31}$ and $\delta^{13}C_{27}$ was used in MixSIAR to estimate the sources of the time-integrated suspended sediment samples collected in the study catchment.

*3.3 Source contributions to watershed sediment loss*

The above results showed that the particle size and organic matter contents have little effect on the carbon isotope contents. The results indicated that for the 12 sediment samples, dry farmland contributed the most (47.4 ± 16.5%), followed by paddy fields and orange orchards, which contributed 32.4 ± 14.7% and orchards 20.2 ± 3.7%, respectively. There are slight differences in the source contributions between the sampling years, but sloping dry farmland was consistently the most important source of suspended sediment. We analyzed the errors associated with the estimated contributions from each source of sediment and found that the standard deviation varied from 12.7%- 24.9%. Here the standard deviation for orchard contributions varied from 12.7%-20%, for paddy fields from 14.3%-24.9%, and for sloping dry farmland from 16.8%-23.6% (Fig. 4).

In 2017, dry farmland contributed 43.4% of the sampled suspended sediment, whereas paddy fields and orange orchards contributed 36.3% and 20.3%, respectively. In 2018, dry

325 farmland contributed 53.0% of sampled sediment, whilst paddy fields and orange orchards
326 contributed 27.0% and 20.0%, respectively. The rice in this area is harvested in late August,
327 and the corresponding contributions of sediment differed before and after the rice harvest.
328 Before the rice harvest, the contribution of the paddy fields was 11.7% higher (37.3%) than that
329 after the harvest (25.6%). After the rice harvest, the sediment contribution from the dry
330 farmlands increased by 41.6% and 55.7%, respectively. During the study period, the sediment
331 contributions from the orange orchards did not change significantly, remaining at ~20%.
332 However, in August when the rice was harvested, paddy fields were the main source of
333 sediment in the study catchment (51.7%), whilst sloping fields and orchards contributed 26.0
334 and 22.3%, respectively. Overall, the results showed a specific pattern: August and October
335 were the peak periods of sediment contributions from paddy fields; September, April and July
336 were the peak periods of sediment delivery from dry farmland, while the contributions from
337 orchards remained comparatively stable throughout the year.
338
339 **4. Discussion**
340 *4.1 Factors affecting the distribution and contents of biomarkers*
341 0A waxy layer often develops on the surface of terrestrial higher plant stems, fruits, petals
342 and leaves to protect plant cells from ultraviolet rays, fungi and insects and maintain water
343 balance. Among them, the epidermal waxy layer of plant leaves has the highest content, and
344 the composition of plant leaf wax is very complex, including long-chain alkanes, alcohols,
345 ketones, acids, lipids and acids (Eglinton and Hamilton, 1967). Plants synthesize organic matter
346 through photosynthesis by absorbing water and $CO_2$ in the surrounding environment, and
347 complex isotope fractionation occurs in the process of biosynthesis. Plants perform
348 photosynthesis by absorbing $CO_2$ in the atmosphere and soil, and there are obvious differences
349 in the carbon isotope of organic matter produced by plants with different photosynthetic
350 pathways (Tipple and Pagani, 2007).
351 Isotope fractionation has nothing to do with organic matter content but only with species
352 and environments. The individual carbon isotope ratios of n-alkanes have been widely used to
353 identify vegetation with different photosynthetic pathways (Sun et al., 2016), including terrestrial
354 higher plants due to photosynthetic pathways ($C_3$/$C_4$). The distribution range of the monomer

355 carbon isotope values of different n-alkanes produced is obviously different. The single carbon
356 isotope ratio of n-alkanes is used the most widely to indicate the change in the relative
357 abundance of $C_3/C_4$ vegetation in a study area.

358 The single carbon isotope of n-alkanes can also be used to explore the environmental
359 conditions of plant growth, such as temperature and humidity changes. Previous studies have
360 shown that the wax carbon isotope values of $C_3$ plants are related to the water supply during
361 photosynthesis (Kohn, 2010; Suh and Diefendorf, 2018; Wang et al., 2018); and, the correlation
362 between carbon isotope changes of $C_4$ plants and water is not obvious. In our small study
363 catchment, orange and rice are $C_3$ vegetation, while corn is $C_4$ vegetation. Orange and rice
364 differ in their n-alkane monomer C isotopes due to the differences in species. In previous
365 research, it has been reported that the monomer carbon isotope content of $C_4$ vegetation is
366 higher than that of $C_3$ vegetation (Chikaraishi and Naraoka, 2003; Meyers, 2003; Bi et al., 2005).
367 Our results also proved this, since dry farmland has the largest carbon isotope ratio, followed
368 by the paddy fields, and orange orchards.

369 The compound-specific $\delta^{13}C$ of n-alkanes exhibited no significant difference between the
370 two particle size fractions and across the whole sampling period, which showed that the
371 monomer carbon isotope of n-alkanes is a good sediment fingerprint. There are several
372 possible explanations for the difference in n-alkane contents between different particle size
373 fractions. Most of the organic carbon is stored in microaggregates (Wang et al., 2017), but the
374 forms of organic matter stored between different particle size fractions are different. The organic
375 components of > 20 μm mainly consist of plant detracts, and the decomposition of these
376 components is slower. Additionally, the morphology of these components is easier to identify in
377 the coarse component than in the fine component; however, the organic constituents in the 20
378 μm component are mainly sapropelized substances with long transformation times (Feller and
379 Beare, 1997; Baldock and Skjemstad, 2000). In addition, fine sediment has a larger specific
380 surface area and can absorb more organic matter. Because of high intensity tillage, land cover
381 and other reasons, dry farmland is more prone to rill erosion, and the particle size selectivity of
382 rill erosion is poor, meaning that both coarse and fine particles will be transported along with
383 runoff (Shi et al., 2012; Wang et al., 2017). Furthermore, different soil erosion processes can
384 cause significant differences in the concentration of organic carbon in sediments by

redistributing sediment particles of different sizes (Nadeu et al., 2011). In our study catchment, soil erosion selectively delivers finer particles of sediment (0-25 μm) to the channel and this selectivity could reflect the intensity of soil erosion. In addition, fine particles may be easier to transport in the paddy fields, while coarser particles mobilized from upstream may be more prone to deposition. However, these results do not prove that individual biomarkers cannot be used as fingerprints, because this study did not analyze their contents in sediment of each particle size fraction, so there may be no significant difference between them overall. In a region with a relatively stable farming system and land use, biomarkers can still be considered as a reliable fingerprinting tracer (Hancock and Revill, 2013; Chen et al., 2016; Chen et al., 2017; Galoski et al., 2019).

*4.2 Land use effects on sediment source contributions*

Our findings do not conflict with conventional knowledge that dry farmlands can often be a principal sediment source. But our results do highlight the dual roles that paddy fields act either as a temporary sediment sink along the delivery continuum or as a secondary proximal suspended sediment source. Paddy fields therefore both trap freshly eroded sediment carried by storm runoff flowing through these part of the catchment, whilst also releasing sediment which is transported to the catchment outlet. By way of comparison, in the Wangjiagou catchment, Fuling, paddy field high ridges are sufficient to intercept excess runoff, reduce runoff speed, and reduce the direct impact of raindrops on the field surface soil (Chen et al., 2019). However, in our investigation, we found that from the end of March to the beginning of May, the study catchment is characterized by rice planting. In the initial stage, the paddy fields would be subjected to high-intensity mechanical cultivation, and coarse particles are broken into finer particles. Since the water storage height is minimal, paddy soils are prone to splash erosion after ploughing. When there is runoff, there is a propensity for fine particles of sediment to be mobilized from the paddy fields (Fig.2). Therefore, in April, paddy fields contributed a large proportion of sediment, as shown in Fig. 4. Any interannual variability in sediment contributions rates may be due to the spatial heterogeneity of rainfall and resultant erosion (Renschler et al., 1999; Renschler and Harbor, 2002).

Primary sediment sources are site-specific and vary occasionally with catchment size and

415 sediment connectivity determined by catchment properties. In the Three Gorges Reservoir area,
416 rice is generally harvested at the end of August. Due to technological innovation, rice is
417 harvested by machines in mountainous areas. Even small machines cause greater damage to
418 the surface than traditional farming operations. Coupled with the recycling of rice stalks, the
419 ground is exposed due to the lack of mulch and erosion therefore increases. In the same way,
420 dry farmlands, where maize is harvested earlier than rice, contributed the most sediment to the
421 study catchment outlet due to the lack of plant cover and the steeper slopes (Chen et al., 2019).
422 Citrus orchards also contributed to suspended sediment loss. As labour costs increase, farmers
423 generally spray herbicides on the ground to kill ground weeds in the orchards to reduce nutrient
424 competition. Despite this, the orchard trees still provide some surface cover, which reduces the
425 splash erosion by raindrops and sediment transport by surface runoff to a certain extent. Here,
426 the retention of the citrus canopy reduces the kinetic energy of raindrops, which is also an
427 important factor in reducing sediment mobilization from the citrus orchards.
428 Monthly sediment contributions from the three sources were also different, which is related
429 to seasonal rainfall, plant growth cycles and human activities. For example, the rice grows well
430 in July, and the dry farmland has already been harvested, meaning that dry farmland soils
431 contributed the most in July, followed by September and October, due to obvious human
432 activities. In April, the plum rain season has just started, and the early rainfall intensity is not
433 high, meaning that only the finest grain size fraction of sediment is transported. When
434 September comes, the rape planting season begins, and dry farmlands and paddy fields are
435 ploughed to sow rape. Bare topsoil, seedlings and mechanical tilling provide ideal conditions
436 for soil erosion in the study catchment at this time. Fortunately, after September, the Three
437 Gorges Reservoir area enters the dry season, and the rain intensity and rainfall amounts are
438 not as severe as the rainy season.
439
440 *4.3 Informative options for soil conservation and sediment management*
441 Since the launch of the Three Gorges Dam, increasing attention has been directed to
442 environmental challenges associated with intensive crop farming on cultivated hillslopes of the
443 surrounding landscapes in the Three Gorges Reservoir Area. Here, the short-distance
444 connectivity for inflowing sediment and associated diffuse pollutants poses a large threat to

445 water quality and ecosystem health of the receiving waters impounded by the reservoir (Fu et
446 al., 2010; Zhang and Lou, 2011; Li et al., 2013b; Xu et al., 2013). Farming has been extended
447 to marginal hillslopes and the cultivation intensity has been intensified over the post-dam period.
448 The sustainability of the local community therefore requires precision land use planning and
449 refined conservation schemes to temper the conflicts between ecosystem conservation and
450 rural livelihood improvement when limited land resource is available. According to the 2019
451 Yangtze River Sediment Bulletin and Chinese national dynamic monitoring of soil erosion, since
452 the reservoir was put into operation in June 2003, the reservoir has accumulated 1.83 billion
453 tons of silt. In 2018, the area of soil erosion in the Three Gorges Reservoir area was 19,200
454 $km^2$, accounting for 33.34% of land. Eutrophication has been a serious problem, and the
455 tributaries are frequently subjected to algal blooms. The statistical evaluation of 649 groups of
456 data from 28 tributaries from 2004 to 2007 shows that the proportion of tributaries suffering light
457 eutrophication is 75% (Wang and Qian, 2009). One of the most important reasons for this is
458 that the sediment in the agricultural catchment surrounding the reservoir area is directly
459 deliveredinto the Yangtze River.

460 Small catchments are the basic unit of sediment yield, sediment transport and soil erosion
461 control. Carrying out comprehensive management of water and soil erosion in small watersheds
462 is the key to reducing the inflow of sediment, improving the ecological environment, and
463 maximising reservoir life span. In order to reduce soil erosion in agricultural catchments, the
464 farming system should be optimized based on increasing the implementation of water and soil
465 conservation measures, such as the promotion of soil virginization technology and changing
466 deep tillage to shallow tillage. This can reduce the artificial fragmentation of soil aggregates.
467 Soils with many water-stable aggregates are more resistant to the formation of soil crusts, have
468 good infiltration, and have less runoff and erosion (Fox et al., 2004). Especially in the case of
469 paddy fields, the implementation of paddy field soil virginization, which can change the micro-
470 topography, thicken the active soil layer for roots and make the capillary pores of the soil
471 connect normally to improve water and air flow represents an important management
472 intervention.

473 In addition, the strategy of returning straw to the field should be promoted. Returning straw
474 to fields can effectively promote microbial activity which degrades the organic components in

475 the straw, increase soil organic matter, optimize the physical structure of the soil, and improve
476 soil fertility (Liu et al., 2014; Hamm et al., 2016; Li et al., 2019). At the same time, straw mulch
477 can intercept rainfall, prevent water volatilization, and form a natural farmland reservoir.
478 Covering the ground with straw can also effectively reduce rainfall kinetic energy, intercept
479 runoff, and greatly reduce soil erosion (Shi et al., 2013). The technology of returning straw to
480 the fields can also greatly increase soil carbon sequestration and reduce greenhouse gases
481 emitted into the atmosphere

482 For the orange orchards, the method of pasture culture is recommended (Li et al., 2013a).
483 The specific measures of this intervention are to interplant *Leguminosae* or *Poaceae* between
484 the rows of orchards or beneath orchards in their entirety, cut them regularly, cover the
485 underside of the trees with the cut stalks, and allow them to decay and decompose naturally
486 (Richardson, 1986). These actions are designed to improve soil structure and soil fertility and
487 reduce soil erosion. Studies on the Three Gorges Reservoir area show that vetch (*vicia villosa*
488 *Roth var.*) is an ideal understory vegetation (Wen et al., 2011; Han et al., 2014). In conjunction
489 with this intervention, herbicides are applied in orchards, which protects the environment. At
490 the same time, as a legume, it can not only fix nitrogen, but also increase soil organic matter
491 after decay (Yang et al., 2020).
492
493 *4.4 Limitations of this study and future research directions*

494 At present, the mainstream biomarkers used in source fingerprinting are mainly fatty acids
495 and n-alkanes (Cooper et al., 2015; Gibbs, 2008; Reiffarth et al., 2016; Mabit et al., 2018;
496 Upadhayay et al., 2018b; Reiffarth et al., 2019). In contrast to fatty acids, n-alkanes are not
497 easily decomposed. Therefore, the use of n-alkane concentrations to track sediment sources
498 has been reported in the literature (Chen et al., 2016; Chen et al., 2017). Monomer carbon
499 isotopes of fatty acids and n-alkanes have been widely used. Decomposition of fatty acids and
500 n-alkanes affects the concentration of total organic matter, but the $\delta^{13}C$ isotopic signature of
501 that compound does not change. Isotopes of short-chain fatty acids, which dissolve in water
502 and migrate with water, were used first (Gibbs, 2008); these biomarkers (C16:0 and C18:0)
503 have applicability to areas with deep soil erosion (C16:0 and C18:0). Tunnel erosion exists in
504 the Loess Plateau, and, therefore, short-chain fatty acids may be a new way to monitor

505 cavitation erosion (Zhu, 2012). Longer-chain fatty acids and n-alkanes are insoluble in water
506 and do not migrate downward with water, so they are more suitable for most areas of severe
507 surface erosion (Reiffarth et al., 2016; Mabit et al., 2018; Upadhayay et al., 2018b; Reiffarth et
508 al., 2019).

509 This study only analyzed the C isotope of n-alkanes. Future work could also include $\delta^2D$
510 isotopes. If fatty acid is used as the fingerprint, the three CHO isotopes can also be tested.
511 Most fingerprint models have an optimal solution, but. the solution set interval of these methods
512 is frequently too small. An optimal solution or a very approximate solution may therefore only
513 represent one possibility for the sediment transport processes of a catchment (Collins et al.,
514 1997a; Collins et al., 2010; Chen et al., 2016; Chen et al., 2017;). In practice, due to the complex
515 interplay of surface soils, land use, rainfall, and hydrology, the same magnitude of sediment
516 loss can be produced by a variety of source contributions, which is the 'black box' model of soil
517 erosion (Borrelli et al., 2021). The MixSIAR model makes the solution set space a normal
518 distribution and considers the likelihood of extreme sediment source contributions. In this case,
519 the sediment source contributions are not restricted which is more consistent with the real
520 situation (Parnell et al., 2010; Xue et al., 2009; Garzon-Garcia et al., 2017). The absolute
521 contributions from the study catchment sources, including paddy fields, were not calculated due
522 to the lack of suspended sediment load monitoring data.

523

524 **5. Conclusion**

525 Exploring the applicability of sediment source fingerprinting in complex landscapes
526 represents a recently identified research priority. Our investigation therefore examined the
527 behaviour of biomarkers (absolute abundance and compound-specific stable isotope ratio of n-
528 alkanes) and their variability among different particle size fractions, and apportioned target time-
529 integrated suspended sediment collected at the study catchment outlet to upstream land-use
530 based sources. The seasonality of the absolute abundance of n-alkanes ($C_{23-33}$) in surface soils,
531 especially in paddy fields, was revealed, which is likely to be related to farming practices, plant
532 growth dynamics and the redox environment. The timing of sampling should be carefully
533 considered when using organic tracers. Repeated sampling could be undertaken as an option
534 to overcome the temporal representativeness of the samples collected. However, the

applicability of compound-specific $\delta^{13}C$ as a conservative tracer to apportion sediment contributions to catchment land-use based sources has been confirmed, as no variability among seasons and particle size fractions was observed. Our fingerprinting with the compound-specific $\delta_{13}C$ of n-alkanes highlights the relative importance of paddy fields as a temporary secondary sediment source, especially during the early Spring when ploughing and rice planting are usually performed. Paddy fields were traditionally assumed to be sediment sinks given the inflow of turbid runoff for irrigation and a major proportion of suspended sediment is likely to be trapped by plant stems.

**Acknowledgements**

This work was supported by the Royal Society Newton International Fellowship (NF161415) awarded to Qiang Tang and supervised by Adrian L. Collins, the Newton International Fellowships Alumni (AL\191023, AL\231030), the Science Fund for Distinguished Young Scholars of Chongqing (cstc2021jcyj-jqX0026), the Special Fund for Youth Team of Southwest University (SWU-XDJH-202306). The contribution by ALC was funded by the UK Research and Innovation–Biotechnology and Biological Sciences Research Council (UKRI-BBSRC) via grant award BB/X010961/1 (Resilient Farming Futures) – specifically work package 2 - BBS/E/RH/230004B; Detecting agroecosystem 'resilience' using novel data science methods.

**References**

Apitz, S.E., 2012. Conceptualizing the role of sediment in sustaining ecosystem services: Sediment-ecosystem regional assessment (SEcoRA). Sci Total Environ, 415: 9-30. DOI:10.1016/j.scitotenv.2011.05.060

Baldock, J.A., Skjemstad, J.O., 2000. Role of the soil matrix and minerals in protecting natural organic materials against biological attack. Organic Geochemistry, 31(7): 697-710. DOI:https://doi.org/10.1016/S0146-6380(00)00049-8

Ben Slimane, A. et al., 2013. Fingerprinting sediment sources in the outlet reservoir of a hilly cultivated catchment in Tunisia. J Soil Sediment, 13(4): 801-815. DOI:DOI 10.1007/s11368-012-0642-6

Bi, X., Sheng, G., Liu, X., Li, C., Fu, J., 2005. Molecular and carbon and hydrogen isotopic

composition of n-alkanes in plant leaf waxes. Organic Geochemistry, 36(10): 1405-1417. DOI:https://doi.org/10.1016/j.orggeochem.2005.06.001

Blake, W.H., Ficken, K.J., Taylor, P., Russell, M.A., Walling, D.E., 2012. Tracing crop-specific sediment sources in agricultural catchments. Geomorphology, 139: 322-329. DOI:DOI 10.1016/j.geomorph.2011.10.036

Borrelli, P. et al., 2021. Soil erosion modelling: A global review and statistical analysis. Science of The Total Environment, 780: 146494. DOI:https://doi.org/10.1016/j.scitotenv.2021.146494

Borrelli, P. et al., 2020. Land use and climate change impacts on global soil erosion by water (2015-2070). Proceedings of the National Academy of Sciences, 117(36): 21994-22001. DOI:10.1073/pnas.2001403117

Chen, F., Fang, N., Shi, Z., 2016. Using biomarkers as fingerprint properties to identify sediment sources in a small catchment. Science of the Total Environment, 557: 123-133.

Chen, F. et al., 2019. Using the sediment fingerprinting method to identify the sediment sources in small catchments with similar geological conditions. Agriculture, Ecosystems and Environment, 286(106655): 1-13. DOI:10.1016/j.agee.2019.106655

Chen, F.X., Fang, N.F., Wang, Y.X., Tong, L.S., Shi, Z.H., 2017. Biomarkers in sedimentary sequences: Indicators to track sediment sources over decadal timescales. Geomorphology, 278: 1-11. DOI:10.1016/j.geomorph.2016.10.027

Chikaraishi, Y., Naraoka, H., 2003. Compound-specific δD–δ13C analyses of n-alkanes extracted from terrestrial and aquatic plants. Phytochemistry, 63(3): 361-371. DOI:https://doi.org/10.1016/S0031-9422(02)00749-5

Collins, A., Walling, D., Leeks, G., 1997a. Source type ascription for fluvial suspended sediment based on a quantitative composite fingerprinting technique. Catena, 29(1): 1-27.

Collins, A.L. et al., 2019. Field scale temporal and spatial variability of delta C-13, delta N-15., TC and TN soil properties: Implications for sediment source tracing. Geoderma, 333: 108-122. DOI:10.1016/j.geoderma.2018.07.019

Collins, A.L. et al., 2017. Sediment source fingerprinting as an aid to catchment management: A review of the current state of knowledge and a methodological decision-tree for end-users. Journal of environmental management, 194: 86-108.

595 DOI:10.1016/j.jenvman.2016.09.075
596 Collins, A.L., Walling, D.E., 2004. Documenting catchment suspended sediment sources:
597 problems, approaches and prospects. Prog Phys Geog, 28(2): 159-196.
598 DOI:10.1191/0309133304pp409ra
599 Collins, A.L., Walling, D.E., Leeks, G.J.L., 1997b. Fingerprinting the origin of fluvial suspended
600 sediment in larger river basins: Combining assessment of spatial provenance and
601 source type. Geogr Ann A, 79A(4): 239-254.
602 Collins, A.L., Walling, D.E., Leeks, G.J.L., 1997c. Source type ascription for fluvial suspended
603 sediment based on a quantitative composite fingerprinting technique. Catena, 29(1): 1-
604 27. DOI:10.1016/s0341-8162(96)00064-1
605 Collins, A.L., Walling, D.E., Webb, L., King, P., 2010. Apportioning catchment scale sediment
606 sources using a modified composite fingerprinting technique incorporating property
607 weightings and prior information. Geoderma, 155(3-4): 249-261.
608 DOI:10.1016/j.geoderma.2009.12.008
609 Cooper, R.J. et al., 2015. Apportioning sources of organic matter in streambed sediments: An
610 integrated molecular and compound-specific stable isotope approach. Sci Total Environ,
611 520: 187-197. DOI:10.1016/j.scitotenv.2015.03.058
612 Du, P.F., Walling, D.E., 2017. Fingerprinting surficial sediment sources: Exploring some
613 potential problems associated with the spatial variability of source material properties.
614 J Environ Manage, 194: 4-15. DOI:10.1016/j.jenvman.2016.05.066
615 Eglinton, G., Hamilton, R.J., 1967. Leaf Epicuticular Waxes. Science, 156(3780): 1322-1335.
616 DOI:10.1126/science.156.3780.1322
617 Fang, H.Y., 2015. Temporal variations of sediment source from a reservoir catchment in the
618 black soil region, Northeast China. Soil and Tillage Research, 153: 59-65.
619 DOI:https://doi.org/10.1016/j.still.2015.04.009
620 Feller, C., Beare, M.H., 1997. Physical control of soil organic matter dynamics in the tropics.
621 Geoderma, 79(1): 69-116. DOI:https://doi.org/10.1016/S0016-7061(97)00039-6
622 Fox, D.M., Bryan, R.B., Fox, C.A., 2004. Changes in pore characteristics with depth for
623 structural crusts. Geoderma, 120(1): 109-120.
624 DOI:https://doi.org/10.1016/j.geoderma.2003.08.010

625 Fox, J.F., Papanicolaou, A.N., 2008. Application of the spatial distribution of nitrogen stable
626 isotopes for sediment tracing at the watershed scale. J Hydrol, 358(1-2): 46-55.
627 DOI:DOI 10.1016/j.jhydrol.2008.05.032
628 Fu, B.J. et al., 2010. Three Gorges Project: Efforts and challenges for the environment. Prog
629 Phys Geog, 34(6): 741-754. DOI:10.1177/0309133310370286
630 Galoski, C.E., Jiménez Martínez, A.E., Schultz, G.B., dos Santos, I., Froehner, S., 2019. Use
631 of n-alkanes to trace erosion and main sources of sediments in a watershed in southern
632 Brazil. Science of The Total Environment, 682: 447-456.
633 DOI:https://doi.org/10.1016/j.scitotenv.2019.05.209
634 Garzon-Garcia, A., Laceby, J.P., Olley, J.M., Bunn, S.E., 2017. Differentiating the sources of
635 fine sediment, organic matter and nitrogen in a subtropical Australian catchment. Sci
636 Total Environ, 575: 1384-1394. DOI:10.1016/j.scitotenv.2016.09.219
637 Gibbs, M.M., 2008. Identifying source soils in contemporary estuarine sediments: A new
638 compound-specific isotope method. Estuar Coast, 31(2): 344-359.
639 DOI:10.1007/s12237-007-9012-9
640 Hamm, A.C. et al., 2016. Bacterial communities of an agricultural soil amended with solid pig
641 and dairy manures, and urea fertilizer. Applied Soil Ecology, 103: 61-71.
642 DOI:https://doi.org/10.1016/j.apsoil.2016.02.015
643 Han, S. et al., 2014. Differences of growth and nutrient accumulation of five leguminous green
644 manure crops intercropping in citrus orchard at Three Gorges Reservoir. Journal of
645 Huazhong Agricultural University, 33(1): 62-66.
646 DOI:10.13300/j.cnki.hnlkxb.2014.01.012
647 Hancock, G.J., Revill, A.T., 2013. Erosion source discrimination in a rural Australian catchment
648 using compound-specific isotope analysis (CSIA). Hydrological Processes, 27(6): 923-
649 932. DOI:10.1002/hyp.9466
650 He, X.B. et al., 2009. Tillage pedogenesis of purple soils in southwestern China. J Mt Sci-Engl,
651 6(2): 205-210. DOI:10.1007/s11629-009-1038-y
652 Huang, D.H. et al., 2019. Using reservoir deposits to quantify the source contributions to the
653 sediment yield in the Black Soil Region, Northeast China, based on the fingerprinting
654 technique. Geomorphology, 339: 1-18. DOI:10.1016/j.geomorph.2019.04.005

655 Jenny, J.-P. et al., 2019. Human and climate global-scale imprint on sediment transfer during
656 the Holocene. P Natl Acad Sci USA, 116(46): 22972-22976.
657 DOI:10.1073/pnas.1908179116
658 Kayvantash, D., Cojan, I., Kissel, C., Franke, C., 2017. Magnetic fingerprint of the sediment
659 load in a meander bend section of the Seine River (France). Geomorphology, 286: 14-
660 26. DOI:10.1016/j.geomorph.2017.02.020
661 Kim, J.K., Onda, Y., Yang, D.Y., Kim, M.S., 2013. Temporal variations of reservoir sediment
662 sources in a small mountainous catchment in Korea. Earth Surf Proc Land, 38(12):
663 1380-1392. DOI:10.1002/esp.3379
664 Kohn, M.J., 2010. Carbon isotope compositions of terrestrial C3 plants as indicators of
665 (paleo)ecology and (paleo)climate. Proceedings of the National Academy of Sciences,
666 107(46): 19691-19695. DOI:10.1073/pnas.1004933107
667 Krein, A., Petticrew, E., Udelhoven, T., 2003. The use of fine sediment fractal dimensions and
668 colour to determine sediment sources in a small watershed. Catena, 53(2): 165-179.
669 DOI:Doi 10.1016/S0341-8162(03)00021-3
670 Li, F. et al., 2013a. Research Advances on Soil and Water Conservation Effect of Pasture-
671 planting in Orchard. Chinese Agricultural Science Bulletin, 29(34): 34-39.
672 Li, K.F., Zhu, C., Wu, L., Huang, L.Y., 2013b. Problems caused by the Three Gorges Dam
673 construction in the Yangtze River basin: a review. Environ Rev, 21(3): 127-135.
674 DOI:10.1139/er-2012-0051
675 Li, X. et al., 2019. Distinct responses of soil fungal and bacterial nitrate immobilization to land
676 conversion from forest to agriculture. Soil Biology and Biochemistry, 134: 81-89.
677 DOI:https://doi.org/10.1016/j.soilbio.2019.03.023
678 Liu, C., Lu, M., Cui, J., Li, B., Fang, C., 2014. Effects of straw carbon input on carbon dynamics
679 in agricultural soils: a meta-analysis. Global Change Biology, 20(5): 1366-1381.
680 DOI:https://doi.org/10.1111/gcb.12517
681 Ludwig, W., Probst, J.L., Kempe, S., 1996. Predicting the oceanic input of organic carbon by
682 continental erosion. Global Biogeochem Cy, 10(1): 23-41. DOI:10.1029/95gb02925
683 Mabit, L. et al., 2018. Novel application of Compound Specific Stable Isotope (CSSI) techniques
684 to investigate on-site sediment origins across arable fields. Geoderma, 316: 19-26.

685 DOI:10.1016/j.geoderma.2017.12.008
686 Martinez-Carreras, N. et al., 2010. Assessment of different colour parameters for discriminating
687 potential suspended sediment sources and provenance: A multi-scale study in
688 Luxembourg. Geomorphology, 118(1-2): 118-129. DOI:DOI
689 10.1016/j.geomorph.2009.12.013
690 Meyers, P.A., 2003. Applications of organic geochemistry to paleolimnological reconstructions:
691 a summary of examples from the Laurentian Great Lakes. Organic Geochemistry, 34(2):
692 261-289.
693 Nadeu, E., de Vente, J., Martínez-Mena, M., Boix-Fayos, C., 2011. Exploring particle size
694 distribution and organic carbon pools mobilized by different erosion processes at the
695 catchment scale. Journal of Soils and Sediments, 11(4): 667-678.
696 DOI:10.1007/s11368-011-0348-1
697 Owens, P.N., Walling, D.E., Leeks, G.J.L., 1999. Use of floodplain sediment cores to investigate
698 recent historical changes in overbank sedimentation rates and sediment sources in the
699 catchment of the River Ouse, Yorkshire, UK. Catena, 36(1-2): 21-47. DOI:Doi
700 10.1016/S0341-8162(99)00010-7
701 Parnell, A.C., Inger, R., Bearhop, S., Jackson, A.L., 2010. Source partitioning using stable
702 isotopes: coping with too much variation. PloS one, 5(3): e9672.
703 DOI:10.1371/journal.pone.0009672
704 Phillips, J.M., Russell, M.A., Walling, D.E., 2000. Time-integrated sampling of fluvial suspended
705 sediment: a simple methodology for small catchments. Hydrol Process, 14(14): 2589-
706 2602. DOI:Doi 10.1002/1099-1085(20001015)14:14<2589::Aid-Hyp94>3.0.Co;2-D
707 Plummer, M., 2003. JAGS: A Program for Analysis of Bayesian Graphical Models using Gibbs
708 Sampling. 3rd International Workshop on Distributed Statistical Computing (DSC 2003);
709 Vienna, Austria, 124.
710 Pulley, S., Foster, I., Collins, A.L., 2017. The impact of catchment source group classification
711 on the accuracy of sediment fingerprinting outputs. J Environ Manage, 194: 16-26.
712 DOI:10.1016/j.jenvman.2016.04.048
713 Pulley, S., Goubet, A., Moser, I., Browning, S., Collins, A.L., 2019. The sources and dynamics
714 of fine-grained sediment degrading the Freshwater Pearl Mussel (Margaritifera

715 margaritifera) beds of the River Torridge, Devon, UK. Sci Total Environ, 657: 420-434.
716 DOI:10.1016/j.scitotenv.2018.11.401
717 Pulley, S., Van der Waal, B., Rowntree, K., Collins, A.L., 2018. Colour as reliable tracer to
718 identify the sources of historically deposited flood bench sediment in the Transkei,
719 South Africa: A comparison with mineral magnetic tracers before and after hydrogen
720 peroxide pre-treatment. Catena, 160: 242-251. DOI:10.1016/j.catena.2017.09.018
721 Reiffarth, D.G., Petticrew, E.L., Owens, P.N., Lobb, D.A., 2016. Sources of variability in fatty
722 acid (FA) biomarkers in the application of compound-specific stable isotopes (CSSIs)
723 to soil and sediment fingerprinting and tracing: A review. Sci Total Environ, 565: 8-27.
724 DOI:10.1016/j.scitotenv.2016.04.137
725 Reiffarth, D.G., Petticrew, E.L., Owens, P.N., Lobb, D.A., 2019. Spatial differentiation of
726 cultivated soils using compound-specific stable isotopes (CSSIs) in a temperate
727 agricultural watershed in Manitoba, Canada. J Soil Sediment, 19(9): 3411-3426.
728 DOI:10.1007/s11368-019-02406-3
729 Renschler, C., Mannaerts, C., Diekkrüger, B., 1999. Evaluating spatial and temporal variability
730 in soil erosion risk—rainfall erosivity and soil loss ratios in Andalusia, Spain. Catena,
731 34(3): 209-225.
732 Renschler, C.S., Harbor, J., 2002. Soil erosion assessment tools from point to regional scales—
733 the role of geomorphologists in land management research and implementation.
734 Geomorphology, 47(2): 189-209.
735 Richardson, A., 1986. The effects of herbicide soil management systems and nitrogen fertilizer
736 on the eating quality of Cox's Orange Pippin apples. Journal of Horticultural Science,
737 61(4): 447-456. DOI:10.1080/14620316.1986.11515725
738 Rowntree, K.M., van der Waal, B.W., Pulley, S., 2017. Magnetic susceptibility as a simple tracer
739 for fluvial sediment source ascription during storm events. J Environ Manage, 194: 54-
740 62. DOI:10.1016/j.jenvman.2016.11.022
741 Shi, Z.H. et al., 2012. Soil erosion processes and sediment sorting associated with transport
742 mechanisms on steep slopes. J Hydrol, 454: 123-130.
743 DOI:10.1016/j.jhydrol.2012.06.004
744 Shi, Z.H. et al., 2013. Effects of Mulch Cover Rate on Interrill Erosion Processes and the Size

Selectivity of Eroded Sediment on Steep Slopes. Soil Science Society of America Journal, 77(1): 257. DOI:10.2136/sssaj2012.0273

Suh, Y.J., Diefendorf, A.F., 2018. Seasonal and canopy height variation in n-alkanes and their carbon isotopes in a temperate forest. Organic Geochemistry, 116: 23-34. DOI:https://doi.org/10.1016/j.orggeochem.2017.10.015

Sun, Q. et al., 2016. An n-alkane and carbon isotope record during the last deglaciation from annually laminated sediment in Lake Xiaolongwan, northeastern China. Journal of Paleolimnology, 56(2): 189-203. DOI:10.1007/s10933-016-9904-4

Tang, Q. et al., 2019. Fingerprinting the sources of water-mobilized sediment threatening agricultural and water resource sustainability: Progress, challenges and prospects in China. Science China Earth Sciences. DOI:10.1007/s11430-018-9349-0

Theuring, P., Collins, A.L., Rode, M., 2015. Source identification of fine-grained suspended sediment in the Kharaa River basin, northern Mongolia. Sci Total Environ, 526: 77-87. DOI:10.1016/j.scitotenv.2015.03.134

Tiecher, T., Caner, L., Minella, J.P.G., Bender, M.A., dos Santos, D.R., 2016. Tracing sediment sources in a subtropical rural catchment of southern Brazil by using geochemical tracers and near-infrared spectroscopy. Soil Till Res, 155: 478-491. DOI:10.1016/j.still.2015.03.001

Tipple, B.J., Pagani, M., 2007. The Early Origins of Terrestrial C4 Photosynthesis. Annual Review of Earth and Planetary Sciences, 35(1): 435-461. DOI:10.1146/annurev.earth.35.031306.140150

Upadhayay, H.R. et al., 2017. Methodological perspectives on the application of compound-specific stable isotope fingerprinting for sediment source apportionment. J Soil Sediment, 17(6): 1537-1553. DOI:10.1007/s11368-017-1706-4

Upadhayay, H.R. et al., 2020. Catchment-wide variations and biogeochemical time lags in soil fatty acid carbon isotope composition for different land uses: Implications for sediment source classification. Org Geochem, 146. DOI:10.1016/j.orggeochem.2020.104048

Upadhayay, H.R. et al., 2018a. Community managed forests dominate the catchment sediment cascade in the mid-hills of Nepal: A compound-specific stable isotope analysis. Sci Total Environ, 637: 306-317. DOI:10.1016/j.scitotenv.2018.04.394

775 Upadhayay, H.R. et al., 2018b. Community managed forests dominate the catchment sediment
776 cascade in the mid-hills of Nepal: A compound-specific stable isotope analysis. Sci
777 Total Environ, 637-638: 306-317. DOI:10.1016/j.scitotenv.2018.04.394
778 Vercruysse, K., Grabowski, R.C., 2018. Using source-specific models to test the impact of
779 sediment source classification on sediment fingerprinting. Hydrol Process, 32(22):
780 3402-3415. DOI:10.1002/hyp.13269
781 Verheyen, D., Diels, J., Kissi, E., Poesen, J., 2014. The use of visible and near-infrared
782 reflectance measurements for identifying the source of suspended sediment in rivers
783 and comparison with geochemical fingerprinting. J Soil Sediment, 14(11): 1869-1885.
784 DOI:10.1007/s11368-014-0938-9
785 Walling, D.E., 2006. Human impact on land–ocean sediment transfer by the world's rivers.
786 Geomorphology, 79(3–4): 192-216.
787 DOI:http://dx.doi.org/10.1016/j.geomorph.2006.06.019
788 Walling, D.E., Fang, D., 2003. Recent trends in the suspended sediment loads of the world's
789 rivers. Global and Planetary Change, 39(1-2): 111-126. DOI:10.1016/s0921-
790 8181(03)00020-1
791 Wang, J. et al., 2018. Disentangling temperature effects on leaf wax n-alkane traits and carbon
792 isotopic composition from phylogeny and precipitation. Organic Geochemistry, 126: 13-
793 22. DOI:https://doi.org/10.1016/j.orggeochem.2018.10.008
794 Wang, Y. et al., 2017. Effects of erosion on the microaggregate organic carbon dynamics in a
795 small catchment of the Loess Plateau, China. Soil and Tillage Research, 174: 205-213.
796 DOI:10.1016/j.still.2017.08.001
797 Wang, Z.-F., Qian, Y.-F., 2009. Frequency and intensity of extreme precipitation events in China.
798 Advances in Water Science, 20(1): 1-9.
799 Wen, M.-x., Shi, X.-j., Nie, Z.-p., Liu, W.-f., Zhou, X.-b., 2011. Effect of summer green manure
800 in Pankan tangerine orchard. Journal of Fruit Science, 28(6): 1077 ～ 1081.
801 DOI:10.13925/j.cnki.gsxb.2011.06.033
802 Wuepper, D., Borrelli, P., Finger, R., 2020. Countries and the global rate of soil erosion. Nature
803 Sustainability, 3(1): 51-55. DOI:10.1038/s41893-019-0438-4
804 Xu, X.B., Tan, Y., Yang, G.S., 2013. Environmental impact assessments of the Three Gorges

Project in China: Issues and interventions. Earth-Sci Rev, 124: 115-125. DOI:10.1016/j.earscirev.2013.05.007

Xue, D. et al., 2009. Present limitations and future prospects of stable isotope methods for nitrate source identification in surface- and groundwater. Water Res, 43(5): 1159-70. DOI:10.1016/j.watres.2008.12.048

Yang, Y.H. et al., 2020. Yield and nutrient concentration in common green manure crops and assessment of potential for nitrogen replacement in different regions of China. Acta Prataculturae Sinica, 29(6): 39-55.

Zhang, Q.F., Lou, Z.P., 2011. The environmental changes and mitigation actions in the Three Gorges Reservoir region, China. Environ Sci Policy, 14(8): 1132-1138. DOI:10.1016/j.envsci.2011.07.008

Zhou, H.P., Chang, W.N., Zhang, L.J., 2016. Sediment sources in a small agricultural catchment: A composite fingerprinting approach based on the selection of potential sources. Geomorphology, 266: 11-19. DOI:10.1016/j.geomorph.2016.05.007

Zhu, T.X., 2012. Gully and tunnel erosion in the hilly Loess Plateau region, China. Geomorphology, 153: 144-155. DOI:10.1016/j.geomorph.2012.02.019

821 **Table 1.** Summary of the sampling scheme for potential sources and time-integrated target
822 suspended sediment samples collected using Phillips traps over a period spanning 2017-2018.

| Catchment-wide potential sediment sources | | | Target suspended sediment samples | Sampling time |
|---|---|---|---|---|
| Orange orchards | Dry croplands | Paddy fields | | |
| 6 | 6 | 6 | | Mar 2017[a] |
| | | | 1 | Jul 2017[b] |
| | | | 4 | Aug 2017 |
| | | | 4 | Oct 2017 |
| 14 | 14 | 14 | 4 | Apr 2018[c] |
| | | | 2 | Sep 2018 |

823 [a] Source samples from paddy fields were taken before ploughing and rice reseeding and the
824 sediment samplers were installed during this field trip.
825 [b] One composite sediment sample was obtained by mixing sediments collected from four
826 independent samplers.
827 [c] Source samples from paddy fields were collected after ploughing and rice reseeding.

**Table 2.** Fingerprint property T tests for the $\delta^{13}C$ n-alkane and n-alkane values measured in the two different absolute particle size fractions (<25 μm and 25-63 μm) of each sediment source category for each sampling year.

| Sampling year | Sediment sources | Independent-samples T test | $\delta^{13}$ n-alkanes | | | | | | n-alkanes | | | | | | | | | | |
|---|---|---|---|---|---|---|---|---|---|---|---|---|---|---|---|---|---|---|---|
| | | | $\delta^{13}C_{23}$ | $\delta^{13}C_{25}$ | $\delta^{13}C_{27}$ | $\delta^{13}C_{29}$ | $\delta^{13}C_{31}$ | $\delta^{13}C_{33}$ | $C_{23}$ | $C_{24}$ | $C_{25}$ | $C_{26}$ | $C_{27}$ | $C_{28}$ | $C_{29}$ | $C_{30}$ | $C_{31}$ | $C_{32}$ | $C_{33}$ |
| 2017 | Orange orchards | F-value | 1.23 | 0.12 | 0.04 | 0.16 | 0.12 | 1.56 | 3.12 | 0.31 | 0.03 | 3.87 | 0.69 | 0.09 | 0.10 | 0.10 | 0.05 | 1.46 | 0.20 |
| | | P-value | 0.54 | 0.25 | 0.85 | 0.99 | 0.33 | 0.83 | 0.78 | 0.46 | 0.67 | 0.63 | 0.98 | 0.80 | 0.72 | 0.74 | 0.81 | 0.95 | 0.58 |
| | Paddy fields | F-value | 0.16 | 3.81 | 0.00 | 2.67 | 0.58 | 0.90 | 1.57 | 1.89 | 1.48 | 5.49 | 0.09 | 1.02 | 0.67 | 2.16 | 6.47 | 0.78 | 0.32 |
| | | P-value | 0.19 | 0.51 | 0.41 | 0.67 | 0.57 | 0.49 | 0.35 | 0.40 | 0.99 | 0.05* | 0.16 | 0.40 | 0.76 | 0.63 | 0.42 | 0.84 | 0.51 |
| | Dry farmland | F-value | 1.32 | 0.55 | 1.73 | 0.03 | 0.01 | 0.00 | 0.60 | 11.25 | 0.01 | 4.97 | 0.30 | 1.28 | 0.91 | 3.36 | 0.70 | 0.00 | 0.32 |
| | | P-value | 0.41 | 0.58 | 0.79 | 0.69 | 0.27 | 0.54 | 0.94 | 0.71 | 0.53 | 0.54 | 0.53 | 0.71 | 0.76 | 0.62 | 0.75 | 0.78 | 0.64 |
| 2018 | Orange orchards | F-value | 2.22 | 2.47 | 1.41 | 1.30 | 0.25 | 2.01 | 14.05 | 20.96 | 12.15 | 15.18 | 3.88 | 12.95 | 3.18 | 11.82 | 1.20 | 1.08 | 0.34 |
| | | P-value | 0.96 | 0.33 | 0.30 | 0.22 | 0.24 | 0.31 | 0.01** | 0.00** | 0.01** | 0.00** | 0.82 | 0.00** | 0.14 | 0.01** | 0.25 | 0.17 | 0.47 |
| | Paddy fields | F-value | 9.36 | 3.34 | 0.64 | 0.01 | 1.16 | 0.92 | 8.52 | 9.64 | 6.36 | 3.27 | 6.21 | 3.52 | 8.75 | 12.42 | 6.36 | 2.18 | 2.93 |
| | | P-value | 0.07 | 0.06 | 0.06 | 0.17 | 0.39 | 0.08 | 0.22 | 0.31 | 0.22 | 0.03* | 0.09 | 0.23 | 0.21 | 0.17 | 0.22 | 0.30 | 0.11 |
| | Dry farmland | F-value | 0.02 | 1.14 | 0.53 | 0.08 | 0.35 | 0.01 | 5.81 | 6.24 | 4.36 | 5.23 | 2.56 | 7.94 | 1.41 | 3.91 | 2.97 | 1.90 | 0.08 |
| | | P-value | 0.97 | 0.56 | 0.86 | 0.75 | 0.99 | 0.92 | 0.25 | 0.18 | 0.36 | 0.23 | 0.33 | 0.13 | 0.46 | 0.98 | 0.38 | 0.50 | 0.80 |

* Significant difference at the 95% credible level.
** Significant difference at the 99% credible level.

832 **Table 3.** T tests for differences between the $\delta^{13}C$ n-alkane signatures (<25 μm fraction) of each

833 sediment source category collected in 2017 and 2018.

| Land use types | Independent-samples T test | Fingerprint property | | | | | |
|---|---|---|---|---|---|---|---|
| | | $\delta^{13}C_{23}$ | $\delta^{13}C_{25}$ | $C^{13}C_{27}$ | $\delta^{13}C_{29}$ | $\delta^{13}C_{31}$ | $\delta^{13}C_{33}$ |
| Orange orchards | F-value | 0.569 | 0.529 | 0.213 | 0.192 | 0.062 | 0.579 |
| | P-value | 0.108 | 0.201 | 0.256 | 0.364 | 0.055 | 0.066 |
| Paddy fields | F-value | 0.613 | 0.564 | 1.418 | 3.046 | 0.612 | 0.019 |
| | P-value | 0.241 | 0.063 | 0.064 | 0.133 | 0.068 | 0.197 |
| Dry farmland | F-value | 13.100 | 26.298 | 9.151 | 1.033 | 0.081 | 0.321 |
| | P-value | 0.322 | 0.987 | 0.348 | 0.061 | 0.405 | 0.277 |

834

835 **Table 4**. Kruskal–Wallis one-way analysis of variance and discrimination function analysis (DFA)

836 results for sediment source discrimination.

| Fingerprint property | Kruskal Wallis | | Minimization of Wilks' lambda | | | | |
|---|---|---|---|---|---|---|---|
| | H-value | P-value | Step | Wilks' lambda | F-value | % source samples classified correctly using individual fingerprint properties | Cumulative % of source samples classified correctly |
| $\delta^{13}C_{33}$ | 31.91 | 0.000** | 1 | 0.419 | 39.57 | 63.3 | 63.3 |
| $\delta^{13}C_{23}$ | 33.52 | 0.000** | 2 | 0.158 | 42.47 | 53.3 | 83.3 |
| $\delta^{13}C_{29}$ | 9.59 | 0.008** | 3 | 0.102 | 39.05 | 51.7 | 88.3 |
| $\delta^{13}C_{31}$ | 33.12 | 0.000** | 4 | 0.089 | 31.70 | 65.0 | 90.0 |
| $\delta^{13}C_{27}$ | 17.31 | 0.000** | 5 | 0.075 | 28.08 | 51.7 | 90.0 |
| $\delta^{13}C_{25}$ | 25.22 | 0.000** | - | - | - | - | - |

837 ** Significant difference at the 99% credible level.
838 "-" indicates the fingerprinting property was excluded from the final composite signature.

**Figure captions**

**Fig. 1.** a. Map showing the spatial extent of the Three Gorges Reservoir extending along the upper Yangtze River and the topography of its surrounding landscapes; b. Remote sensing image generated by a drone flying over the study catchment in the middle reaches that directly drains to the reservoir, and; c. Land use in the study catchment.

**Fig. 2.** Images of the study landscape. a. dry croplands; b. paddy fields at the end of April, showing a low water level meaning that the soil disturbed by mechanical ploughing is prone to splash erosion; c. orange orchards converted from dry croplands for over 15 years, and; d. time-integrated suspended sediment sampler installed near the study catchment outlet.

**Fig. 3.** The biomarker results for the different absolute particle size fractions of the potential sediment sources.

**Fig. 4**. Sediment source contributions during 2017 and 2018. The error bars indicate the standard deviations (SD).

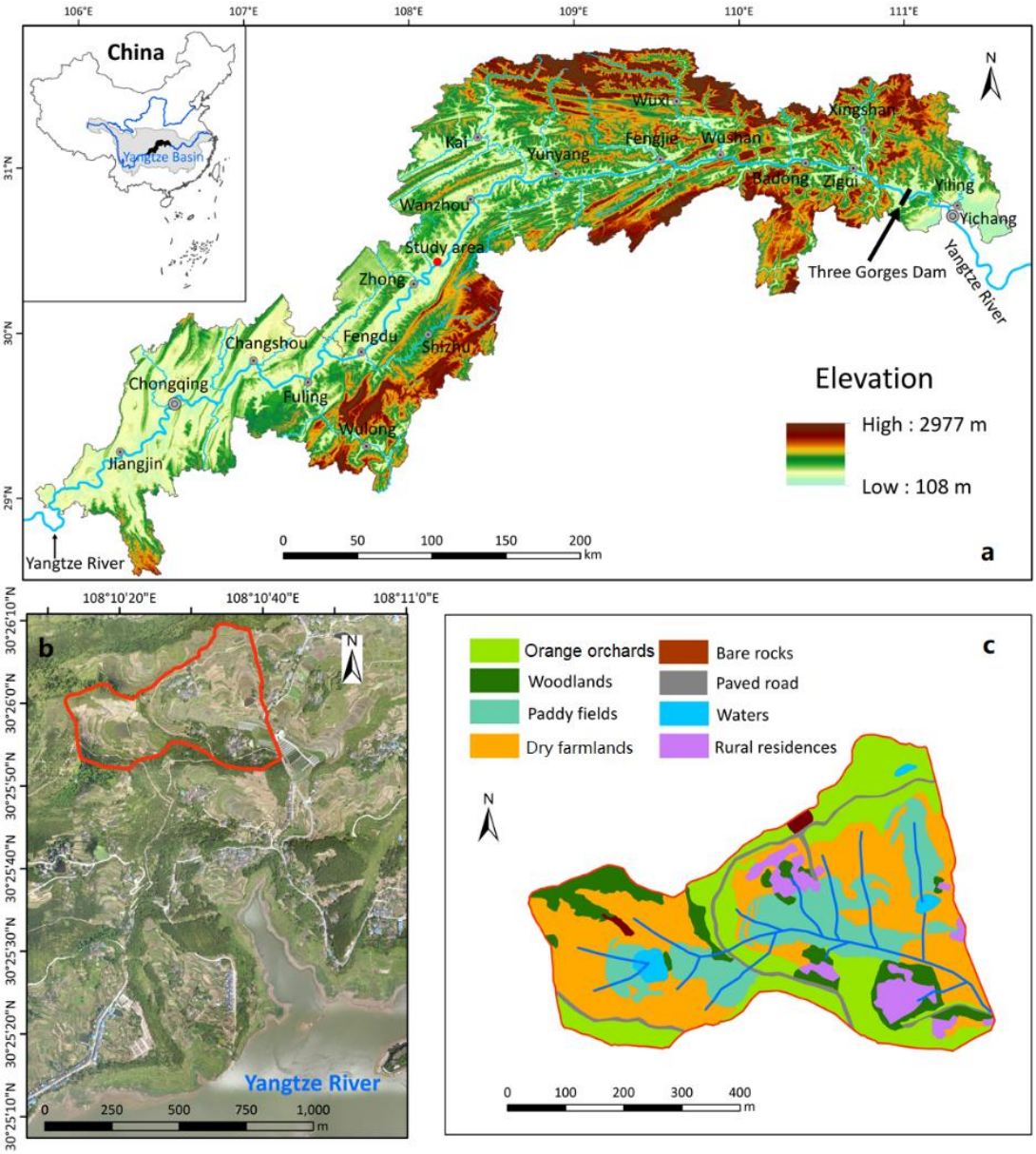


853 **Figure 1**

854

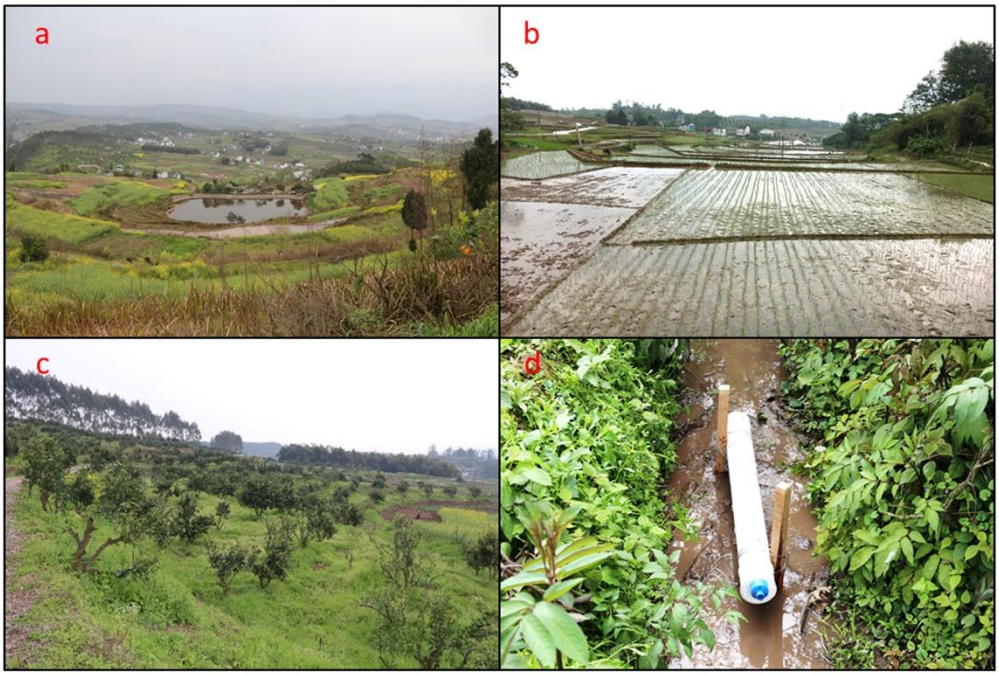


855 **Figure 2**

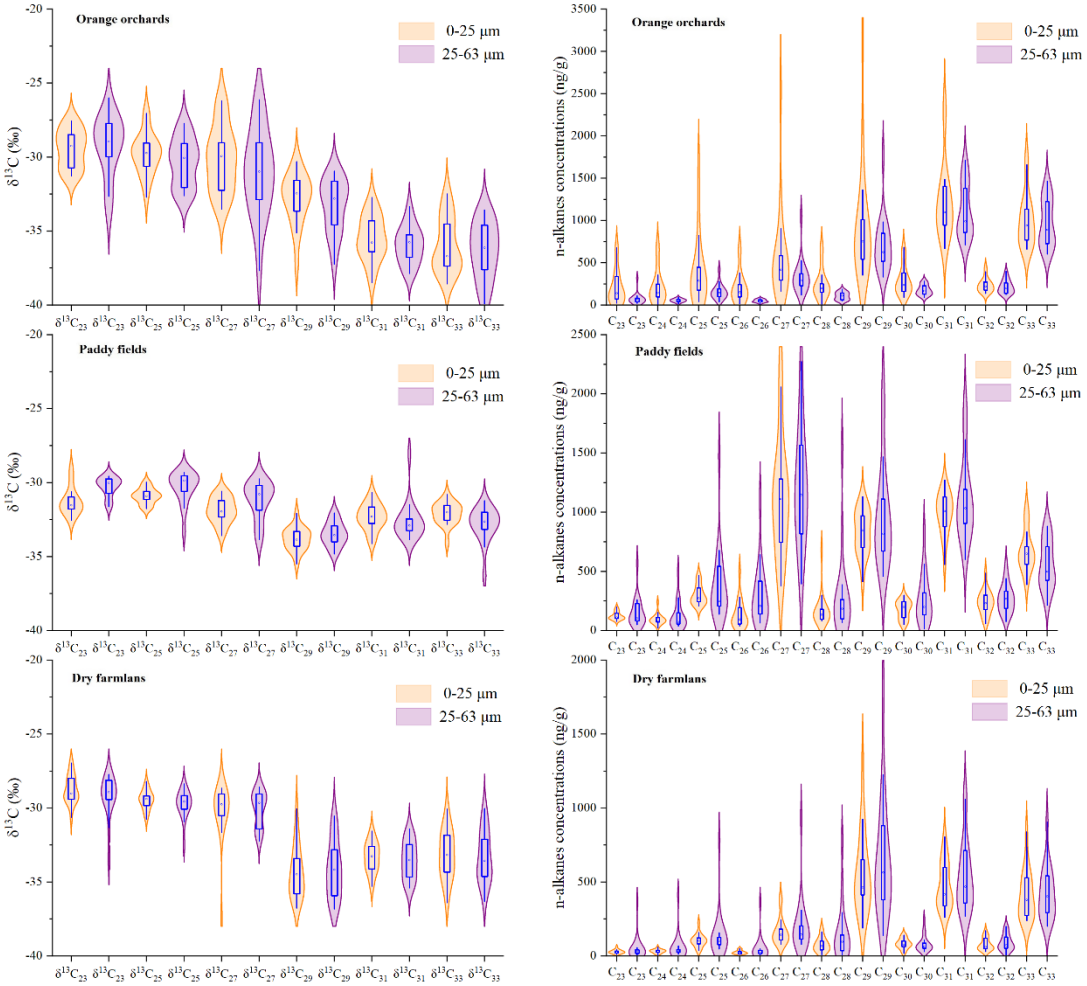


856
857 **Figure 3**

858

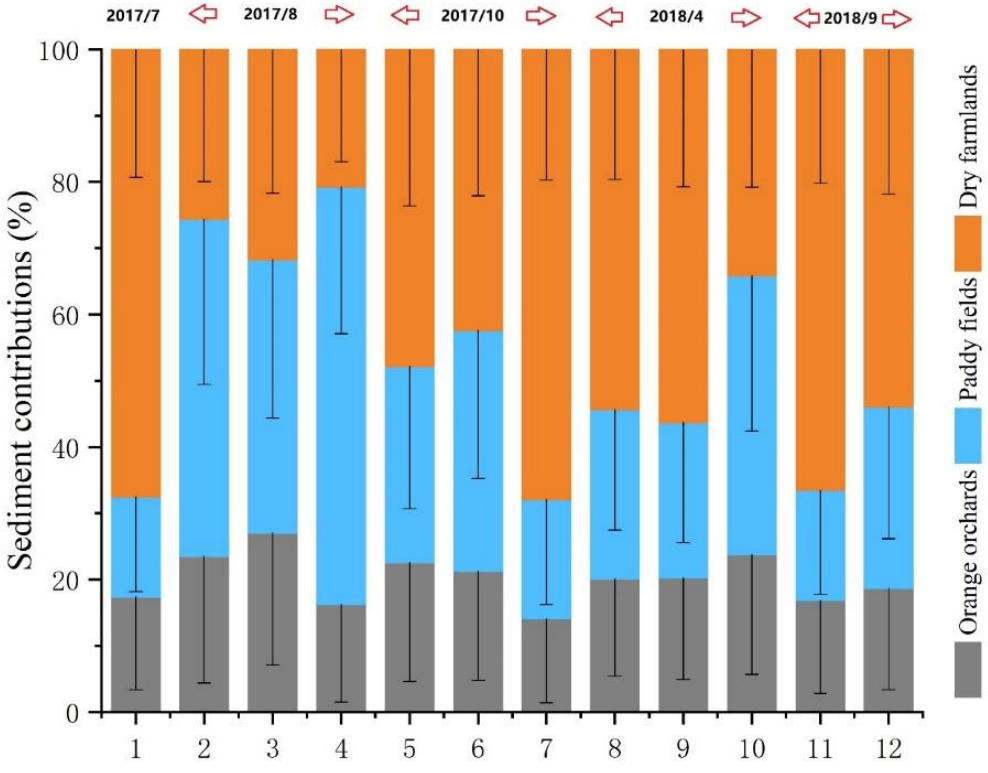
2017/7
2017/8
2017/10
2018/4
2018/9
Sediment contributions (%)
100
80
60
40
20
0
1
2
3
4
5
6
7
8
9
10
11
12
Dry farmlands
Paddy fields
Orange orchards

**Figure 4**